SF2A 2013
L. Cambrésy, F. Martins, E. Nuss and A. Palacios (eds)

MAGNETIC FIELDS IN OLD SUPERNOVA REMNANTS

A. Gusdorf[1], T. Hezareh[2], S. Anderl[3] and H. Wiesemeyer[2]

Abstract. We review the motivations and methods for studying magnetic fields in relatively old supernova remnants (SNRs), such as W28, W44, 3C 391, and IC 443. We first explain the common methods of determination of interstellar magnetic fields through measurements of polarization levels in cosmic dust and spectral line emission. We then present the methods used in our study, i.e., shock modelling of molecular line emission, and application of non-Zeeman circular polarization of spectral lines. We finalize with the new perspectives of this study.

Keywords: ISM: supernova remnants – Physical data and processes: magnetic fields – Shock waves – Submillimeter: ISM – ISM: individual objects: W28, W44, IC443, & 3C391 – cosmic rays.

1 Supernova remnants and magnetic fields

Supernovae play a key role in the energy input in the interstellar medium (ISM). At their latest stage of evolution, i.e., at the so-called 'supernova remnant' (SNR) stage, these objects drive shocks that compress, accelerate and heat the ambient gas. Strong infrared and sub-millimeter spectral line emission is observed from such sources, as presented in this review: W28, W44, IC 443, 3C 391. This emission can be used to study the physical and chemical processes in shock environments and to constrain shock model parameters for such regions. Subsequently, general conclusions can be drawn on the effects of SNRs on the ambient ISM (Gusdorf et al. 2013). These effects include the contribution of SNRs to the energetic balance of galaxies, their input of turbulence, and triggered second generation star formation. Moreover, a detailed analysis of the molecular emission in SNRs can also contribute to the interpretation for the observed γ-ray emission, and hence a better understanding of the acceleration mechanisms and population of cosmic rays.

Among the shock parameters that can be constrained through the modelling of molecular line emission in SNRs, the magnetic field strength is of particular importance: it strongly influences the type of shock (C- or J-type) propagating in the ISM, hence the associated cooling processes and ultimately the amount of energy that is radiated away. Furthermore, the magnetic field strength is required to determine the proportion of electrons and hadrons in the cosmic ray population detectable around SNRs. Indeed, both electrons and hadrons generate γ-ray emission through interactions with the dense ISM. The analysis of high-energy spectra is consequently not sufficient to disentangle their contributions. However, relativistic electrons also interact with the magnetic field, giving rise to synchrotron emission, observable from radio to X-ray wavelengths. The proportion of electrons in the cosmic rays population can hence be determined if the magnetic field strength is known, and then be confirmed by the interpretation of γ-rays spectra.

In this brief contribution, we will review the 'classical' determinations of the magnetic field strength in the ISM, and then present the methods our team uses, based on shock modelling of molecular emission and the interpretation of the polarization of spectral lines of the CO molecule.

[1] LERMA, UMR 8112 du CNRS, Observatoire de Paris, École Normale Supérieure, 24 rue Lhomond, F75231 Paris Cedex 05, France
[2] Max Planck Institut für Radioastronomie, Auf dem Hügel 69, 53121 Bonn, Germany
[3] Argelander Institut für Astronomie, Universität Bonn, Auf dem Hügel 71, 53121 Bonn, Germany

2 Observational methods for measuring magnetic fields

Interstellar magnetic fields cause the emission of dust particles and atomic and molecular gas species to be polarized. Measurement of this (usually weak) polarized emission is the key to determine the orientation and strength of the ambient magnetic field. For example, in the submillimeter regime, the thermal radiation from non-spherical dust particles becomes linearly polarized perpendicular to the magnetic field lines. A dust polarization map therefore reveals the projection of the magnetic field orientation in the plane of the sky (e.g., Hildebrand et al. 1999). Recent developments in intricate calculations of the dispersion of polarization vectors have led to determination of physical parameters such as the turbulent correlation length in a cloud, the turbulent-to-large-scale magnetic field strength ratio, and the plane-of-the-sky component of the magnetic field strength (Hildebrand et al. 2009, Houde et al. 2009, 2011, 2013).

Magnetic fields can also cause molecular spectral lines to be linearly polarized (Goldreich & Kylafis 1981). Molecules align with the ambient magnetic field and the presence of a source of anisotropy in the medium, such as velocity gradients parallel or perpendicular to the magnetic field, or an external anisotropic radiation, causes a population imbalance in the magnetic sublevels. This causes the emission from these molecules to be linearly polarized. Depending on which sublevel population dominates, the detected linear polarization can be parallel or perpendicular to the magnetic field (Cortes et al. 2005).

Finally, the only direct way of obtaining the strength of magnetic fields is through the Zeeman effect. More precisely, the line-of-sight component of the field can be obtained by measuring the net circular polarization of a molecular spectral line with a significant Zeeman splitting coefficient (e.g., Crutcher et al. 1999, or Claussen et al. 1997, 1999 for applications to SNRs environments). In rare cases where the Zeeman splitting is directly resolved between right- and left- circularly polarized spectra, the total field strength can be constrained (see Hoffman et al. 2005 for measurements in the W28 SNR).

3 Our Work

3.1 Shock modelling

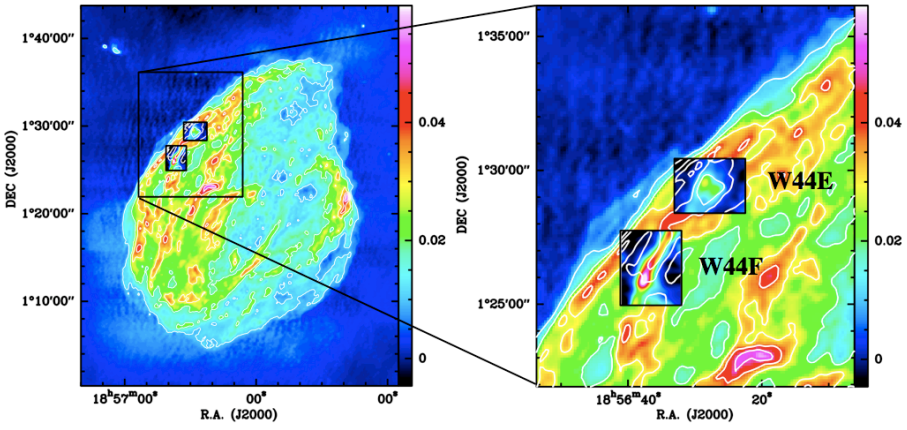

Fig. 1. An example of the regions investigated in our shock modelling studies: W44, Anderl et al., in prep. **Left:** wide-field radio continuum image at 1442.5 MHz, with wedge in units of Jy/beam, from Giacani et al. (1997). **Right:** zoom in the regions W44E and W44F. The insets consist of our CO (6-5) maps, where the intensity is integrated across the velocity range of the shocked gas. The white contours on both panels are radio continuum in steps of 10 mJy.

Our first method of determination of magnetic fields is based on the comparison of molecular line observations with shock models. Dense clumps associated with SNR shells are selected for observations of molecular lines that best trace the shocked gas: CO, a very good density and temperature probe for its abundance and dipole moment and H_2, for its quadrupole transitions at very high temperatures. Several spectral lines of these molecules are targeted, and the corresponding integrated intensities (for CO) or column densities (for H_2, whose lines are naturally optically thin) are used in a so-called 'spectral line energy distribution' (or SLED, for CO) or excitation diagram (for H_2). These observed quantities are then systematically compared to a grid of modelled ones, generated by a state-of-the-art, one-dimensional shock code, designed to simulate the propagation of

stationary C- or J-type shocks, or of non-stationary CJ ones in a dense molecular medium. Such a comparison was first performed in the G knot of SNR IC 443 Cesarsky et al. (1999), using the rotational lines of H_2 observed by ISO. Since then, it has been applied to shocks associated with star formation (e.g. Gusdorf et al. 2011), and again to SNRs such as W28 and 3C 391 (Gusdorf et al. 2012, Gusdorf et al., in prep), and W44 (Anderl et al., in prep). Figure 1 shows an example of the regions where our analysis has been conducted in the SNR W44.

Our goal is to constrain input parameters of our shock models, including pre-shock density $n_{\rm H}$, shock velocity $v_{\rm s}$, age, and type, and the magnetic field strength in the direction perpendicular to the propagation of the considered shock wave. The magnetic field strength determines the type of shock driven in the ISM. In a poorly magnetized medium, the shock corresponds to the propagation of a strong discontinuity in the medium (in temperature, for instance), hence the name 'J-type' (J for Jump) shock. On the contrary, in a strongly magnetized medium, the magnetic field component perpendicular to the shock smoothens this discontinuity, and the maximum temperature and gas compression are attenuated, hence the name 'C-type' (C for Continuous) shock. Both the H_2 excitation diagram and CO SLED reflect this temperature and density differences, hence the suitability of our method to constrain shock parameters. As our shock models self-consistently computes the abundance of over 125 molecules, we can use additional molecules in a similar way to lift a possible degeneracy. So far, the magnetic field values perpendicular to the shock direction yielded by this method have always been found compatible with those inferred from Zeeman measurements from (post-shock) OH masers.

3.2 Application for Non-Zeeman circular polarization observations

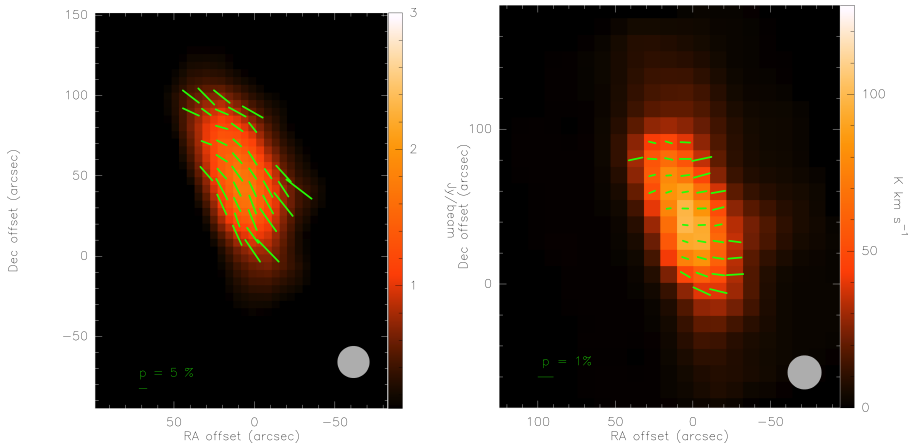

Fig. 2. Left: Dust polarization map of clump G in SNR IC 443 obtained at the APEX telescope. The polarization vectors are perpendicular to the magnetic field lines. **Right:** Polarization map of CO (1–0) in clump G in SNR IC 443 obtained at the IRAM 30-m telescope. The combination of the dust and CO linear polarization maps resulted in the realization of linear-to-circular polarization conversion in CO emission. The cause of this polarization conversion is suggested to be a change of magnetic field orientation in this clump, along the line of sight. From Hezareh et al. (2013).

In a recent study, Hezareh et al. (2013) compared linear polarization maps of dust continuum (observed with the APEX telescope) with polarization maps of CO (2–1) and (1–0) transitions in clump G in SNR IC 443. The dust polarization map shows levels of polarization of up to 10%, and shows a magnetic field orientation perpendicular to the long axis of the source (Figure 1a). The linear polarization maps of CO also reveal polarization levels consistent with what is expected from the Goldreich-Kylafis effect. However, no 0° or 90° difference was seen between the polarization angles of the two sets of maps.

In addition to linear polarization in CO, circular polarization was also detected for the same molecular transitions, with intrinsic levels of up to 0.5–1%. The detected circular polarization is not caused by the Zeeman effect, as the splitting factor for the CO molecule is 4 orders of magnitude smaller than that of the routinely observed molecules like CN and OH. Hezareh et al. (2013) showed that these observations are a result of linear-to-circular polarization conversion in CO emission. The cause of this conversion is explained in a physical model based on anisotropic resonant scattering (Houde et al. 2013). In this model, linearly polarized CO emission (through the Goldreich-Kylafis effect for instance), propagates through the depth of the clump along the line-of-sight, and strikes similar species of molecules in the foreground layer (somewhere in the outer

envelope). If the magnetic field orientation has changed with respect to the deeper regions of the source, then the CO molecules will absorb this linearly polarized emission at the transition frequency to a virtual state and re-emit it via anisotropic resonant scattering with a phase shift between its scattered amplitudes. This phase shift between the orthogonally polarized components of the scattered emission can cause a transformation of linear to circular polarization.

Hezareh et al. (2013) measured this phase shift in their observations and used its value at every pixel of the CO maps to convert the observed circularly polarized flux into linear and recalculate the CO polarization vectors to obtain the anticipated consistency with the dust polarization vectors. Houde et al. (2013) showed that according to this physical model, the amount of the observed phase shift between the components of the incoming signal in each pixel of the maps is a function of the excitation temperature and column density of the observed species, and also the square of the strength of the plane-of-the-sky component of the magnetic field. If the anisotropic resonant scattering model is proven to be the indeed the cause of the confirmed polarization transformation, then a beam-per-beam method for the determination of the magnetic field strength in the plane of the sky will be made possible. This application will be investigated in Hezareh et al., in prep.

4 Conclusion

One of the most significant shortcomings of our shock model is its simple, one-dimensional shock geometry. This means we always assume that the molecular emission comes from a shock layer parallel to the line of sight and seen face-on. Although this method takes a step further compared to more simple approaches (such as 'slab' LVG techniques), the complexity of the observed regions ideally requires multi-dimensional computations, that are very time demanding for current processors. To overcome this difficulty, Kristensen et al. (2008) and Gustafsson et al. (2010) have developed a pseudo-multidimensional model, where one-dimensional shock layers are stitched on curves or surfaces of shocks. The major drawback of this technique is the lack of knowledge on the orientation of the magnetic field with respect to the adopted curves or surfaces. If the anisotropic resonant scattering model discussed in Section 3.2 is indeed causing the linear-to-circular conversion of the observed line polarization, then the combination of dust and CO polarization maps will open a new way to not only trace the changes in magnetic field orientation in extended sources along the line of sight, but also estimate the field strength at several positions in the source and considerably restrict the number of free parameters associated with the current pseudo-multidimensional shock models.

A. Gusdorf acknowledges support by the grant ANR-09-BLAN-0231-01 from the French *Agence Nationale de la Recherche* as part of the SCHISM project. S. Anderl acknowledges support by the DFG SFB 956, the International Max Planck Research School (IMPRS) for Astronomy and Astrophysics, and the Bonn-Cologne Graduate School of Physics and Astronomy.

References

Cesarsky, D., Cox, P., Pineau des Forêts, G., et al. 1999, A&A, 348, 945
Claussen, M. J., Frail, D. A., Goss, W. M., & Gaume, R. A. 1997, ApJ, 489, 143
Claussen, M. J., Goss, W. M., Frail, D. A., & Desai, K. 1999, ApJ, 522, 349
Cortes, P. C., Crutcher, R. M., & Watson, W. D. 2005, ApJ, 628, 780
Crutcher, R. M., Troland, T. H., Lazareff, B., Paubert, G., & Kazès, I. 1999, ApJ, 514, L121
Giacani, E. B., Dubner, G. M., Kassim, N. E., et al. 1997, AJ, 113, 1379
Goldreich, P. & Kylafis, N. D. 1981, ApJ, 243, L75
Gusdorf, A., Anderl, S., Güsten, R., et al. 2012, A&A, 542, L19
Gusdorf, A., Giannini, T., Flower, D. R., et al. 2011, A&A, 532, A53
Gustafsson, M., Ravkilde, T., Kristensen, L. E., et al. 2010, A&A, 513, A5
Hezareh, T., Wiesemeyer, H., Houde, M., Gusdorf, A., & Siringo, G. 2013, A&A, 558, A45
Hildebrand, R. H., Dotson, J. L., Dowell, C. D., Schleuning, D. A., & Vaillancourt, J. E. 1999, ApJ, 516, 834
Hildebrand, R. H., Kirby, L., Dotson, J. L., Houde, M., & Vaillancourt, J. E. 2009, ApJ, 696, 567
Hoffman, I. M., Goss, W. M., Brogan, C. L., & Claussen, M. J. 2005, ApJ, 627, 803
Houde, M., Hezareh, T., Jones, S., & Rajabi, F. 2013, ApJ, 764, 24
Houde, M., Rao, R., Vaillancourt, J. E., & Hildebrand, R. H. 2011, ApJ, 733, 109
Houde, M., Vaillancourt, J. E., Hildebrand, R. H., Chitsazzadeh, S., & Kirby, L. 2009, ApJ, 706, 1504
Kristensen, L. E., Ravkilde, T. L., Pineau Des Forêts, G., et al. 2008, A&A, 477, 203